Nuclear Physics B133 (1978) 13–37

CHARGED HADRON MULTIPLICITIES AND INCLUSIVE π^- DISTRIBUTIONS IN INELASTIC ep SCATTERING

C.K. CHEN [*], J. KNOWLES, D. MARTIN, J.M. SCARR, I.O. SKILLICORN and K. SMITH
University of Glasgow, Glasgow, UK

P. JOOS, A. LADAGE, H. MEYER [**], P. STEIN [***], G. WOLF and S. YELLIN [§]
Deutsches Elektronen-Synchrotron DESY, Hamburg, Germany

C. BENZ, G. DREWS, D. HOFFMANN [§§], J. KNOBLOCH [§§§], W. KRAUS, H. NAGEL, E. RABE, C. SANDER, W.-D. SCHLATTER [§§§], H. SPITZER and K. WACKER [**]
II. Institut für Experimentalphysik der Universität Hamburg, Hamburg, Germany

Received 4 November 1977

Electroproduction of hadrons is studied in the kinematic region $W < 2.8$ GeV and $0.3 < Q^2 < 1.4$ GeV^2 using the DESY streamer chamber. Prong cross sections, charged-particle multiplicities and inclusive π^- distributions are presented. The average charged multiplicity is found to be independent of Q^2 in the Q^2 range studied here; however it is lower than in photoproduction. The fraction of forward π^- is found to be significantly less in electroproduction than in photoproduction. The $\langle p_T^2 \rangle$ for inclusive π^- is, for all x values, similar to that found in photoproduction.

1. Introduction

In this paper we report the inclusive features of hadronic final states produced by inelastic scattering of 7.2 GeV electrons on protons. The data cover the kinematic range $0.3 < Q^2 < 1.4$ GeV^2 and $W < 2.8$ GeV. ($-Q^2$ is the mass squared of the

[*] Now at Argonne National Laboratory, Argonne, Ill., USA.
[**] Now at Bergische Universität Wuppertal, Germany.
[***] On leave of absence from Cornell University, Ithaca, N.Y., USA.
[§] Now at University of California, Santa Barbara, California, USA.
[§§] Now at Technische Hochschule Aachen, III. Physikalisches Institut A, Aachen, Germany
[§§§] Now at CERN, Geneva, Switzerland.

exchanged virtual photon and W is the effective mass of all the final state hadrons.) This range is intermediate between photoproduction at $Q^2 = 0$, where the interactions resemble hadronic processes, and the scaling region at $W > 2$ GeV and $Q^2 > 1$ GeV^2, where inelastic ep scattering data have given indications for point-like constituents of the proton. We also know that s-channel resonances are excited in the region $W < 1.8$ GeV whereas for $W > 1.8$ GeV diffractive processes like ρ and ω production are important [1,2]. It is our aim to study the Q^2 and W dependence of the inclusive features of the data in these regions.

In sect. 2 a brief description of the apparatus and the treatment of the events is given. Sect. 3 presents the Q^2 and W dependence of the simplest overall features of the interactions, namely, the topological cross sections and the mean charged hadron multiplicity. The inclusive momentum spectra for $\gamma_V + p \to \pi^- + X$ are presented in sect. 4. In sect. 5 we discuss which channels are responsible for the observed differences in mean charged particle multiplicity between $Q^2 = 0$ and $Q^2 = 0.3$ GeV^2. The results are summarised in sect. 6.

This paper reports our final results. Preliminary results based on a smaller data sample have been given in ref. [3].

2. Experimental procedure

2.1. Experimental setup

A detailed description of the experimental setup and the event analysis has been given in refs. [3,4]. An electron beam of 7.2 GeV was directed onto a 9 cm long liquid hydrogen target inside the DESY streamer chamber. The streamer chamber allows the observation of the outgoing charged particles with nearly 4π acceptance.

Table 1
Resolution in W (σ_W) for unfitted events

W(GeV)	Q^2 (GeV^2)	σ_W (GeV)
1.65	0.4	±0.082
	0.65	±0.074
	1.1	±0.071
2.0	0.4	±0.055
	0.65	±0.041
	1.1	±0.037
2.6	0.4	±0.019
	0.65	±0.018
	1.1	±0.013

The resolution was determined from a Monte Carlo program for non-radiating events.

A pair of trigger arms, composed of scintillation counters, lucite Čerenkov counters, and lead-scintillator sandwich shower counters, identified the scattered electrons and triggered the streamer chamber. For the data reported here the lucite Čerenkov counter inserted into the shower counter near shower maximum allows for an improved rejection of pion triggers [4] compared to earlier data [3]. Furthermore, a proportional wire chamber with x, y readout was added to each of the trigger arms. This improved the measurement of the momentum vector of the scattered electrons by more than a factor of two and resulted in a considerably better mass resolution σ_W for small values of W. Typical values of σ_W are given in table 1 *.

2.2. The event sample

The event sample reported here was obtained from a data run with approximately $2 \cdot 10^{12}$ electrons hitting the target. The event analysis was similar to that of bubble chamber experiments. Scanning losses were very small ($\lesssim 1\%$) and have been neglected. Correction factors for events which were not successfully measured depend slightly on prong number and amount to 1.01, 1.03 and 1.06 for 1-, 3- and 5-prong events respectively. One-prong events have been measured on ~30% of the film only. The number of prongs always refers to the number of charged hadronic tracks only.

Since we are concerned here with inelastic electron scattering, events fitting elastic electron-proton scattering are not included in the data sample. The elastic events which do not make a 4C fit due to radiation were removed by eliminating 2-prong events which satisfied the following criteria with a χ^2 probability >1%: The missing mass was consistent with zero and the missing momentum vector was consistent with either the incident or outgoing electron direction. The fraction of events removed from the total event sample by this procedure is 7% at $W \approx 1.6$ GeV falling to 3.5% at $W \approx 2.5$ GeV. Events with visible strange particle decays, amounting to ~1% of the data, are not included in the analysis **.

Each event in the resulting sample is weighted to correct for acceptance, radiation effects, and smearing in Q^2 and W due to measurement errors. The radiation corrections were generated separately for each topology using as input a fit to the total inelastic electron-proton cross section of ref. [6] together with the fractional prong cross sections of our earlier runs [3]. The Monte Carlo generated distributions agree with the observed Q^2, W distributions of the raw events and the input fractional prong cross sections are consistent with the results presented below. To indicate the

* The resolution in Q^2 varies from $\sigma = \pm 0.01$ GeV^2 at $Q^2 = 0.4$ GeV^2 to $\sigma = \pm 0.02$ GeV^2 at $Q^2 = 1$ GeV^2 (independent of W).

** This procedure has also been applied in inclusive photoproduction results [5]. It should be noted that because of the different decay volumes the procedure is not equivalent in the two experiments. In the photoproduction experiment the fraction of events with visible strange particle decays was ~6% (at $W = 2.45$ GeV). We estimate from the number of visible K^- decays that our π^- inclusive spectra contain a K^- contamination of less than 8.5%.

Table 2
Acceptance and radiation corrections at center of Q^2, W bins

Q^2(GeV^2) $\langle Q^2 \rangle$	W(GeV) $\langle W \rangle$	Acceptance	Radiation and measurement error correction		
			1-prong	3-prong	5-prong
0.3–0.5 (0.4)	1.5–1.8 (1.65)	0.235	1.06	1.36	1.41
	1.8–2.2 (2.0)	0.245	0.90	1.15	1.30
	2.2–2.8 (2.5)	0.230	0.78	1.04	1.20
0.5–1.4 (0.9)	1.5–1.8 (1.65)	0.190	1.12	1.25	1.35
	1.8–2.2 (2.0)	0.175	1.00	1.19	1.30
	2.2–2.8 (2.5)	0.150	0.89	1.10	1.26

The radiation correction includes a −7% correction for vertex and propagator effects (see ref. [4] for details). The statistical uncertainty of the radiation correction is ±0.05 (from the Monte Carlo generation).

size of the corrections table 2 gives the acceptance and the radiative correction at the central values of the Q^2, W bins used below. The tabulated radiative corrections include the effects of smearing due to measurement errors.

Table 3 shows the topological distribution of the raw events for three intervals of W. About 7.5% of events have an even number of hadronic prongs and are assumed

Table 3
Numbers of raw events in the interval $0.3 < Q^2 < 1.4$ GeV^2 (in addition we have 171 events with visible strange particle decay)

No. of prongs	$1.1 < W < 1.5$ GeV	$1.5 < W < 1.8$ GeV	$1.8 < W < 2.2$ GeV	$2.2 < W < 2.8$ GeV
0 [a]	64	65	61	38
1 [a]	2249	1679	1477	1003
2	117	229	378	332
3	856	2179	3561	4054
4	6	10	42	56
5	2	13	57	286
6	0	0	1	8
7	0	0	0	3
Sum	3294	4175	5577	5780

[a] From 30% of the film. Elastic events ep → ep are excluded.

to have a track hidden by flares or the target. The three-prong sample includes events from the channel $ep \to ep\pi^+\pi^-$, observed as 2-prong events, for which a missing track has been reconstructed by means of a 1C fit (see subsect. 4.3 of ref. [4]). These events amount to 3% of all events at $W \approx 1.6$ and 1.5% of all events at $W \approx 2.5$ GeV. The remaining even prong events have been added to the next higher topology for the purpose of the mean charged multiplicity and prong cross section determinations. The 4-prong events have been carefully examined for spurious tracks to avoid the possibility of a 3-prong plus a spurious electron or positron track being taken as a 5-prong with a lost track. This check is particularly important in the case of 4-prong events, since the number of 3-prong events is considerably greater than the number of 5-prong events.

For the inclusive distributions, the total number of tracks has been corrected for missing tracks for each topology, which is equivalent to assuming that the missing tracks have the same distribution as the observed tracks of the same topology *; 0.3% of the events have a charge imbalance greater than one unit and have been neglected.

Above $W = 2.6$ GeV where the trigger electron energy is low ($E' \leq 4.1$ GeV) a correction for erroneous pion triggers by photoproduction events has been estimated. The resulting corrections are less than the statistical errors and have not been applied.

For the data presented here we use measured (unfitted) variables for all events (with the exception of fig. 7a, see subsect. 4.1). This procedure is consistent with our method for the determination of the inclusive radiative corrections where the effect of kinematic fitting is not considered.

3. Mean charged multiplicity and fractional prong cross sections

In this section we present the dependence of the mean charged multiplicity and the fractional prong cross sections on the photon "mass" Q^2 and the hadronic c.m.s. energy W.

The fractional prong cross section is defined as $\sigma_n(Q^2, W)/\sigma_{\text{tot}}(Q^2, W)$, where σ_n is the cross section for events with n charged hadronic prongs, $\sigma_{\text{tot}} = \Sigma_n \sigma_n$. The mean charged multiplicity is then

$$\langle n_{\text{ch}} \rangle = \sum_n n\sigma_n/\sigma_{\text{tot}} .$$

All cross sections presented below are virtual photon cross sections averaged over the quoted Q^2, W regions. The prong cross sections are given by

$$\sigma_n(Q^2, W) \propto \frac{1}{\Delta Q^2 \Delta W} \sum_i \frac{Wt_i(n, Q^2, W)}{\Gamma_i(Q^2, W)},$$

* The tracks recovered by a 1C fit for channel $ep \to ep\pi^+\pi^-$ have x and $p_\perp$ distributions similar to those from the observed tracks of this channel.

Table 4
Charged multiplicities and fractional prong cross sections as a function of Q^2 for different W intervals

$1.3 < W < 1.5$ GeV $\quad \langle W \rangle = 1.4$ GeV				
Q^2 (GeV^2)	$\langle n_{ch} \rangle$	σ_1/σ_{tot}	σ_3/σ_{tot}	σ_{tot} (μb) [a]
0.3–0.4	1.49 ± 0.03	0.76 ± 0.02	0.24 ± 0.02	135.7 ± 5.8
0.4–0.5	1.44 ± 0.03	0.78 ± 0.02	0.22 ± 0.02	137.8 ± 6.3
0.5–0.6	1.37 ± 0.03	0.82 ± 0.02	0.18 ± 0.02	101.2 ± 6.0
0.6–0.7	1.43 ± 0.05	0.79 ± 0.02	0.21 ± 0.02	102.6 ± 7.4
0.7–1.0	1.39 ± 0.04	0.80 ± 0.02	0.20 ± 0.02	81.4 ± 5.7
1.0–1.4	1.41 ± 0.10	0.79 ± 0.05	0.21 ± 0.05	50.2 ± 7.7
$1.5 < W < 1.8$ GeV $\quad \langle W \rangle = 1.65$ GeV				
Q^2 (GeV^2)	$\langle n_{ch} \rangle$	σ_1/σ_{tot}	σ_3/σ_{tot}	σ_{tot} (μb) [a]
0.3–0.4	1.69 ± 0.03	0.66 ± 0.02	0.34 ± 0.02	149.4 ± 4.7
0.4–0.5	1.72 ± 0.03	0.64 ± 0.02	0.36 ± 0.02	132.8 ± 4.4
0.5–0.6	1.76 ± 0.04	0.62 ± 0.02	0.38 ± 0.02	108.4 ± 4.5
0.6–0.7	1.72 ± 0.05	0.65 ± 0.02	0.35 ± 0.02	92.5 ± 5.2
0.7–1.0	1.67 ± 0.04	0.67 ± 0.02	0.33 ± 0.02	82.1 ± 4.2
1.0–1.4	1.75 ± 0.09	0.63 ± 0.05	0.37 ± 0.05	61.6 ± 6.5

The above total cross sections were determined by normalising to the total inelastic ep cross section measured in a single arm experiment [6]. The above errors are statistical only. An additional 8% uncertainty is due to normalisation and radiative corrections.

$1.8 < W < 2.2$ GeV $\quad \langle W \rangle = 2.0$ GeV					
Q^2 (GeV^2)	$\langle n_{ch} \rangle$	σ_1/σ_{tot}	σ_3/σ_{tot}	σ_5/σ_{tot}	σ_{tot} (μb) [a]
0.0 [b]	2.32 ± 0.06	0.34	0.645	0.015	141
0.3–0.4	2.06 ± 0.03	0.49 ± 0.02	0.50 ± 0.02	0.014 ± 0.004	93.6 ± 2.6
0.4–0.5	2.05 ± 0.03	0.49 ± 0.02	0.50 ± 0.02	0.014 ± 0.004	89.8 ± 2.5
0.5–0.6	2.07 ± 0.04	0.48 ± 0.02	0.51 ± 0.02	0.014 ± 0.004	74.6 ± 2.8
0.6–0.7	2.14 ± 0.05	0.45 ± 0.03	0.53 ± 0.03	0.018 ± 0.005	68.9 ± 3.2
0.7–1.0	2.05 ± 0.04	0.49 ± 0.02	0.49 ± 0.02	0.015 ± 0.005	61.5 ± 2.5
1.0–1.4	1.96 ± 0.09	0.53 ± 0.05	0.46 ± 0.04	0.010 ± 0.005	51.1 ± 4.7
$2.2 < W < 2.8$ GeV $\quad \langle W \rangle = 2.5$ GeV					
Q^2 (GeV^2)	$\langle n_{ch} \rangle$	σ_1/σ_{tot}	σ_3/σ_{tot}	σ_5/σ_{tot}	σ_{tot} (μb) [a]
0.0 (ref. [8])	2.77 ± 0.06	0.18 ± 0.01	0.75 ± 0.02	0.068 ± 0.003	124.3 ± 3.0
0.3–0.4	2.42 ± 0.04	0.35 ± 0.02	0.60 ± 0.02	0.053 ± 0.007	79.3 ± 2.5
0.4–0.5	2.48 ± 0.04	0.33 ± 0.02	0.60 ± 0.02	0.065 ± 0.007	73.0 ± 2.0
0.5–0.6	2.42 ± 0.05	0.36 ± 0.02	0.57 ± 0.02	0.067 ± 0.008	68.0 ± 2.5
0.6–0.7	2.37 ± 0.06	0.37 ± 0.03	0.57 ± 0.03	0.055 ± 0.009	62.8 ± 2.9
0.7–1.0	2.50 ± 0.05	0.32 ± 0.02	0.61 ± 0.02	0.069 ± 0.009	52.3 ± 2.0
1.0–1.4	2.48 ± 0.10	0.31 ± 0.04	0.64 ± 0.04	0.052 ± 0.016	40.3 ± 3.2

[a] Excluding events with visible strange particle decay.
[b] Interpolated values from refs. [8,9].

Table 5
Charged multiplicities and fractional prong cross sections as a function of W for $0.3 < Q^2 < 1.4$ GeV^2 (ϵ is the polarization parameter)

$0.3 < Q^2 < 1.4$ GeV^2		$\langle Q^2 \rangle = 0.78$ GeV^2			
W (GeV)	$\langle \epsilon \rangle$	$\langle n_{ch} \rangle$	σ_1/σ_{tot}	σ_3/σ_{tot}	σ_5/σ_{tot}
1.1–1.2	0.99	1.00 ± 0.00	1.00	0.0	
1.2–1.3	0.99	1.06 ± 0.01	0.97 ± 0.01	0.03 ± 0.01	
1.3–1.4	0.99	1.34 ± 0.03	0.83 ± 0.02	0.17 ± 0.02	
1.4–1.5	0.98	1.48 ± 0.04	0.76 ± 0.02	0.24 ± 0.02	
1.5–1.6	0.98	1.66 ± 0.04	0.67 ± 0.02	0.33 ± 0.02	
1.6–1.7	0.97	1.67 ± 0.05	0.67 ± 0.02	0.33 ± 0.02	0.002 ± 0.001
1.7–1.8	0.96	1.83 ± 0.05	0.59 ± 0.02	0.41 ± 0.02	0.005 ± 0.002
1.8–1.9	0.95	1.93 ± 0.05	0.54 ± 0.03	0.44 ± 0.03	0.011 ± 0.004
1.9–2.0	0.94	2.00 ± 0.06	0.51 ± 0.03	0.47 ± 0.03	0.013 ± 0.004
2.0–2.1	0.93	2.11 ± 0.06	0.46 ± 0.03	0.53 ± 0.03	0.015 ± 0.004
2.1–2.2	0.91	2.11 ± 0.07	0.46 ± 0.04	0.52 ± 0.04	0.016 ± 0.004
2.2–2.3	0.89	2.27 ± 0.08	0.39 ± 0.04	0.58 ± 0.04	0.024 ± 0.005
2.3–2.4	0.87	2.36 ± 0.08	0.37 ± 0.04	0.59 ± 0.04	0.045 ± 0.013
2.4–2.5	0.85	2.47 ± 0 06	0.32 ± 0.03	0.63 ± 0.03	0.049 ± 0.013
2.5–2.6	0.82	2.56 ± 0.07	0.29 ± 0.03	0.66 ± 0.03	0.056 ± 0.009
2.6–2.7	0.78	2.59 ± 0.07	0.29 ± 0.03	0.62 ± 0.03	0.090 ± 0.017
2.7–2.8	0.74	2.57 ± 0.09	0.34 ± 0.03	0.55 ± 0.03	0.110 ± 0.018

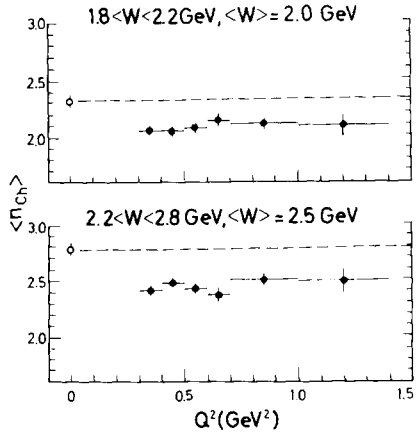

Fig. 1. The mean charged hadron multiplicity, $\langle n_{ch} \rangle$, as a function of Q^2 for $1.8 < W < 2.2$ and $2.2 < W < 2.8$ GeV. The photoproduction data at $Q^2 = 0$ are from ref. [8].

where Wt is the acceptance and radiation correction factor, Γ is the usual [7] virtual photon flux factor and the summation is over the events in the kinematical region $\Delta Q^2 \times \Delta W$

$$\Gamma = \frac{\alpha}{4\pi} \frac{W}{M^2 E^2 Q^2} \frac{W^2 - M^2}{1 - \epsilon} ,$$

where ϵ, the virtual photon polarisation parameter, is given by

$$\frac{1}{\epsilon} = 1 + 2 \frac{\nu^2 + Q^2}{4EE' - Q^2} ,$$

with E, E' = initial, final electron energies,
$\nu = E - E'$,
M = proton mass.

Tables 4 and 5 list the data discussed in this section.

Fig. 1 shows $\langle n_{ch} \rangle$ as a function of Q^2 for $\langle W \rangle$ = 2.0 and 2.5 GeV. The photoproduction points (at $Q^2 = 0$) are taken from the data of ref. [8], the point at 2.0 GeV being an interpolated value. The electroproduction data are *independent of* Q^2 over the range 0.3–1.4 GeV^2 but are ~12% lower than the photoproduction points.

Fig. 2 shows the fractional prong cross sections, σ_n/σ_{tot}, for $\langle W \rangle$ = 2.5 GeV and the photoproduction data of ref. [8]. Again, the electroproduction data are inde-

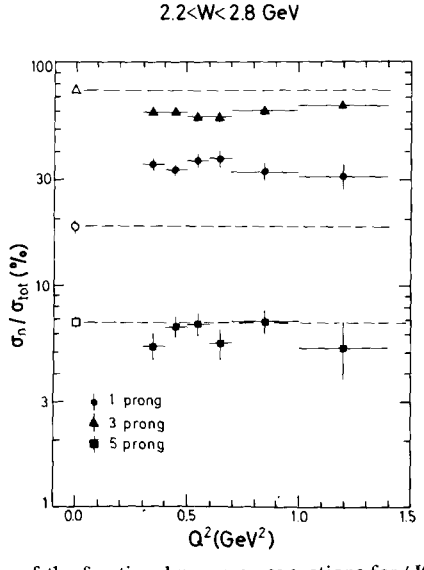

Fig. 2. The Q^2 dependence of the fractional prong cross sections for $\langle W \rangle$ = 2.5 GeV. The photoproduction data (open points) are from ref. [8] (W = 2.48 GeV). The dashed lines indicate the level of the photoproduction data.

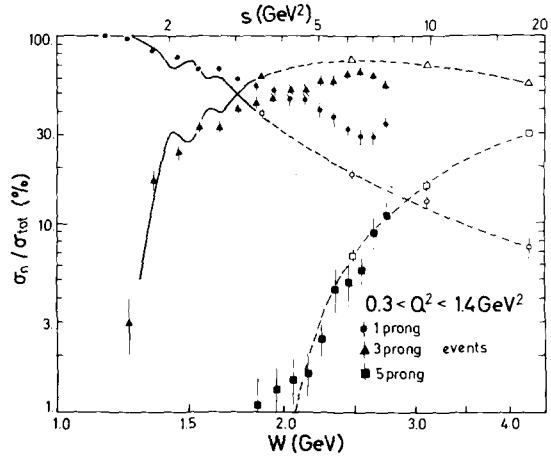

Fig. 3. Fractional prong cross sections as a function of $s = W^2$, averaged over $0.3 < Q^2 < 1.4$ GeV^2 The curves are interpolations through photoproduction results, taken from ref. [8] (open points) for $s > 3$ GeV^2 and determined from the data of refs. [9,10] for $s < 3$ GeV^2.

pendent of Q^2 for $0.3 < Q^2 < 1.4$ GeV^2. While the 5-prong fractional cross section is consistent with the photoproduction value, the 1- and 3-prong fractional cross sections differ significantly. The 7-prong cross section is negligible at this energy.

Since the electroproduction data show no Q^2 dependence in the region $0.3 < Q^2 < 1.4$ GeV^2, we present in figs. 3 and 4 our data averaged over this range ($\langle Q^2 \rangle = 0.78$ GeV^2).

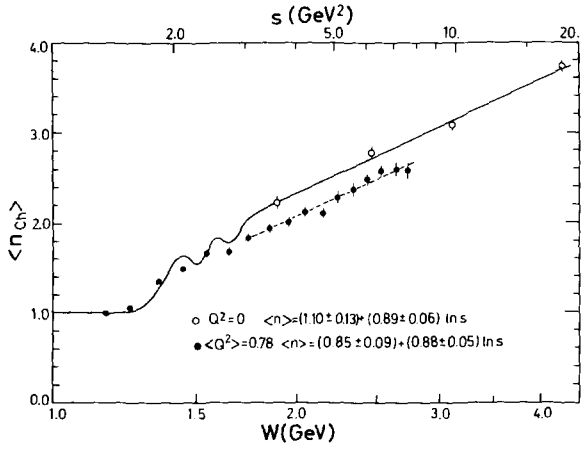

Fig. 4. The mean charged hadron multiplicity, $\langle n_{ch} \rangle$, as a function of $s = W^2$ averaged over $0.3 < Q^2 < 1.4$ GeV^2. The full curve shows an interpolation through photoproduction results (open points) using data as for fig. 3. The dashed curve represents a fit to our data.

Fig. 3 shows the fractional prong cross sections, averaged over Q^2, as a function of $s = W^2$. For comparison, photoproduction data are also shown; the dashed lines are hand drawn curves through the photoproduction data of ref. [8] (open points), while the full curves for $s < 3$ GeV^2 have been calculated from the total cross section [9] and the 3-prong cross section [10]. (The $\geqslant$5-prong cross sections are negligible for $s < 3$ GeV^2.) The 5-prong fractional cross section shows similar behaviour for $Q^2 = 0$ and $\langle Q^2 \rangle = 0.78$ GeV^2 in contrast to the 1- and 3-prong fractional cross sections which display a different W dependence for the photoproduction and electroproduction data. Fig. 4 shows $\langle n_{ch} \rangle$ as a function of $s = W^2$. For $s > 3$ GeV^2 our data are consistent with a logarithmic behaviour (dashed curve):

$$\langle n_{ch} \rangle = (0.85 \pm 0.09) + (0.88 \pm 0.05) \ln s .$$

For comparison the open points are the photoproduction data of ref. [8] which can be fitted for $s > 3$ GeV^2 (full line) by

$$\langle n_{ch} \rangle = (1.10 \pm 0.13) + (0.89 \pm 0.06) \ln s .$$

Below $s = 3$ GeV^2 the full line has been obtained from photoproduction data in the same way as the corresponding curves in fig. 3. The value of $\langle n_{ch} \rangle$ for photoproduction is seen to be ~12% higher than for electroproduction throughout the range 3 <

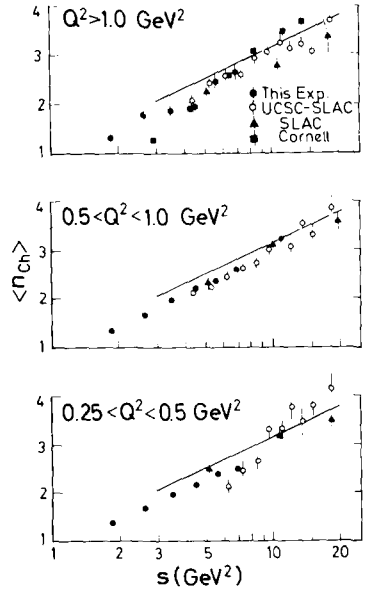

Fig. 5. Comparison of electroproduction data for the s dependence of $\langle n_{ch} \rangle$ for three regions of Q^2, • this experiment, ○ UCSC-SLAC [11], ▲ SLAC [12] and ■ Cornell [13]. The solid lines are a fit to photoproduction data of ref. [8] using $\langle n_{ch} \rangle = 1.10 \pm 0.89 \ln s$.

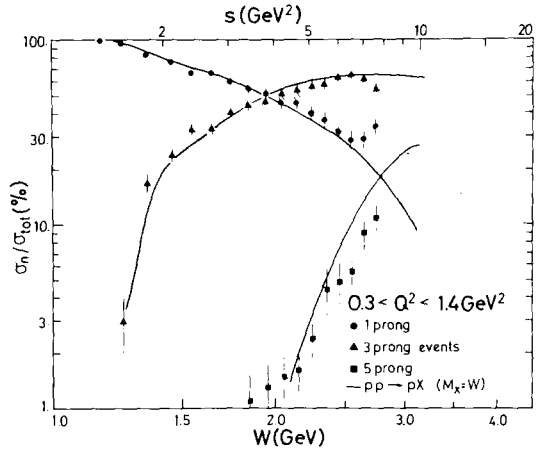

Fig. 6. The fractional prong cross sections from this experiment (data points) as a function of W compared to those obtained from pomeron + proton → X (full curves) as a function of M_X, the mass of X, obtained from the reaction pp → pX [14].

$s < 8$ GeV^2 reflecting the behaviour of the 1- and 3-prong fractional cross sections shown in fig. 3. In the resonance region, below $s = 3$ GeV^2 the agreement between photoproduction and electroproduction is closer; however, limited resolution in our experiment at low W (see table 1) precludes the observation of resonance structure similar to that seen in photoproduction (figs. 3, 4).

Fig. 5 shows a comparison of our data for $\langle n_{ch} \rangle$ with the results of other electroproduction experiments [11–13] for three intervals of Q^2. The agreement, in general, is good.

We now compare our multiplicity distributions with data on the pomeron-proton interaction where the total hadronic charge involved is the same as in electroproduction. The pomeron-proton cross sections have been derived from the reaction pp → p + X (anything) [14 *]. The selection method is based on the rapidity distribution, so as to obtain events with one of the protons diffractively scattered. In fig. 6 the ratio σ_n/σ_{tot}, for prong multiplicity $n = 1, 3, 5$, is shown as a function of W for the hadronic events (curves) and for our electroproduction data (full points). (In the hadronic data the mass of X is equivalent to W.) For all channels the hadronic and electroproduction data show a similar energy dependence and cross section ratio. This suggests that there is little difference between the overall features of the virtual photon-proton and the pomeron-proton interactions.

In conclusion, the mean charged multiplicities and fractional prong cross sections show no dependence on the photon mass for $Q^2 > 0.3$ GeV^2. The same observation

* The charged multiplicities are from a private communication of the authors.

Table 6a

$$F(x, p_\perp^2) = \frac{1}{\pi\sigma_{tot}} \frac{E^*}{p^*_{max}} \frac{\Delta^2\sigma}{\Delta x \, \Delta p_\perp^2} \quad \text{for} \quad 1.8 < W < 2.2 \text{ GeV}$$ [a)]

$p_\perp^2((\text{GeV}/c)^2)$	$-1.0 < x < -0.3$		$-0.3 < x < -0.1$		$-0.1 < x < 0.1$	
	$0.3 < Q^2 < 0.5$	$0.5 < Q^2 < 1.4$	$0.3 < Q^2 < 0.5$	$0.5 < Q^2 < 1.4$	$0.3 < Q^2 < 0.5$	$0.5 < Q^2 < 1.4$
0.0 –0.04	0.140 ± 0.015	0.121 ± 0.020	0.45 ± 0.04	0.75 ± 0.11	0.78 ± 0.05	0.92 ± 0.09
0.04–0.08	0.080 ± 0.012	0.102 ± 0.023	0.29 ± 0.04	0.38 ± 0.07	0.47 ± 0.04	0.44 ± 0.07
0.08–0.12	0.063 ± 0.011	0.065 ± 0.014	0.17 ± 0.03	0.24 ± 0.06	0.29 ± 0.04	0.17 ± 0.03
0.12–0.16	0.034 ± 0.009	0.030 ± 0.012	0.13 ± 0.03	0.16 ± 0.07	0.16 ± 0.03	0.15 ± 0.04
0.16–0.20	0.024 ± 0.007	0.021 ± 0.007	0.078 ± 0.022	0.112 ± 0.035	0.100 ± 0.025	0.089 ± 0.025
0.20–0.24	0.021 ± 0.007	0.022 ± 0.009	0.100 ± 0.027	0.077 ± 0.022	0.095 ± 0.026	0.097 ± 0.026
0.24–0.32	0.016 ± 0.005	0.021 ± 0.014	0.053 ± 0.014	0.050 ± 0.016	0.053 ± 0.014	0.108 ± 0.028
0.32–0.40	0.007 ± 0.003	0.019 ± 0.013	0.049 ± 0.015	0.035 ± 0.015	0.057 ± 0.016	0.014 ± 0.009
0.40–0.60	0.002 ± 0.001	0.001 ± 0.001	0.008 ± 0.004	0.006 ± 0.004	0.008 ± 0.004	0.017 ± 0.007
0.60–0.80		0.001 ± 0.001				0.004 ± 0.003
$p_\perp^2((\text{GeV}/c)^2)$	$0.1 < x < 0.3$		$0.3 < x < 0.7$		$0.7 < x < 1.0$	
	$0.3 < Q^2 < 0.5$	$0.5 < Q^2 < 1.4$	$0.3 < Q^2 < 0.5$	$0.5 < Q^2 < 1.4$	$0.3 < Q^2 < 0.5$	$0.5 < Q^2 < 1.4$
0.0 –0.04	0.65 ± 0.05	0.68 ± 0.08	0.35 ± 0.03	0.24 ± 0.05	0.31 ± 0.04	0.26 ± 0.08
0.04–0.08	0.43 ± 0.04	0.39 ± 0.07	0.25 ± 0.03	0.17 ± 0.03	0.21 ± 0.04	0.14 ± 0.03
0.08–0.12	0.32 ± 0.04	0.27 ± 0.06	0.21 ± 0.03	0.21 ± 0.03	0.16 ± 0.03	0.13 ± 0.07
0.12–0.16	0.22 ± 0.04	0.12 ± 0.06	0.14 ± 0.02	0.102 ± 0.019	0.026 ± 0.012	0.032 ± 0.014
0.16–0.20	0.16 ± 0.03	0.14 ± 0.06	0.11 ± 0.02	0.076 ± 0.020	0.054 ± 0.019	0.038 ± 0.016
0.20–0.24	0.096 ± 0.026	0.096 ± 0.031	0.13 ± 0.02	0.052 ± 0.015	0.009 ± 0.009	0.003 ± 0.003
0.24–0.32	0.053 ± 0.015	0.039 ± 0.014	0.043 ± 0.010	0.020 ± 0.009	0.000 ± 0.004	0.003 ± 0.002
0.32–0.40	0.057 ± 0.016	0.016 ± 0.009	0.007 ± 0.004	0.018 ± 0.006	0.004 ± 0.004	
0.40–0.60	0.020 ± 0.006	0.009 ± 0.003	0.011 ± 0.003	0.004 ± 0.002	0.002 ± 0.002	
0.60–0.80		0.005 ± 0.005		0.013 ± 0.013		

[a)] In this and the following tables the average Q^2 is $\langle Q^2 \rangle = 0.4$ GeV^2 for the interval $0.3 < Q^2 < 0.5$ GeV^2 and $Q^2 = 0.9$ GeV^2 for $0.5 < Q^2 < 1.4$ GeV^2

Table 6b

$F(x, p_\perp^2) = \frac{1}{\pi\sigma_{\text{tot}}} \frac{E^*}{p^*_{\text{max}}} \frac{\Delta^2\sigma}{\Delta x\, \Delta p_\perp^2}$ for $2.2 < W < 2.8$ GeV

$p_\perp^2((\text{GeV}/c)^2)$	$-1.0 < x < -0.3$		$-0.3 < x < -0.1$		$-0.1 < x < 0.1$	
	$0.3 < Q^2 < 0.5$	$0.5 < Q^2 < 1.4$	$0.3 < Q^2 < 0.5$	$0.5 < Q^2 < 1.4$	$0.3 < Q^2 < 0.5$	$0.5 < Q^2 < 1.4$
0.0 –0.04	0.050 ± 0.008	0.083 ± 0.029	0.53 ± 0.04	0.52 ± 0.05	1.03 ± 0.05	1.06 ± 0.09
0.04–0.08	0.054 ± 0.009	0.060 ± 0.020	0.42 ± 0.04	0.37 ± 0.06	0.60 ± 0.05	0.65 ± 0.09
0.08–0.12	0.046 ± 0.009	0.019 ± 0.007	0.25 ± 0.03	0.25 ± 0.05	0.30 ± 0.06	0.38 ± 0.06
0.12–0.16	0.028 ± 0.007	0.056 ± 0.026	0.16 ± 0.03	0.18 ± 0.03	0.33 ± 0.05	0.30 ± 0.07
0.16–0.20	0.030 ± 0.007	0.044 ± 0.018	0.16 ± 0.03	0.076 ± 0.025	0.17 ± 0.03	0.11 ± 0.06
0.20–0.24	0.015 ± 0.006	0.011 ± 0.005	0.049 ± 0.019	0.070 ± 0.021	0.12 ± 0.03	0.17 ± 0.06
0.24–0.32	0.015 ± 0.004	0.016 ± 0.006	0.056 ± 0.013	0.041 ± 0.012	0.101 ± 0.019	0.095 ± 0.024
0.32–0.40	0.010 ± 0.004	0.024 ± 0.011	0.043 ± 0.013	0.079 ± 0.034	0.057 ± 0.014	0.069 ± 0.018
0.40–0.60	0.004 ± 0.001	0.004 ± 0.002	0.014 ± 0.005	0.018 ± 0.007	0.020 ± 0.005	0.022 ± 0.006
0.60–0.80	0.001 ± 0.001		0.006 ± 0.004	0.007 ± 0.004	0.004 ± 0.003	0.008 ± 0.005
0.80–1.00	0.002 ± 0.001		0.004 ± 0.003	0.003 ± 0.002	0.002 ± 0.002	0.002 ± 0.002
$p_\perp^2((\text{GeV}/c)^2)$	$0.1 < x < 0.3$		$0.3 < x < 0.7$		$0.7 < x < 1.0$	
	$0.3 < Q^2 < 0.5$	$0.5 < Q^2 < 1.4$	$0.3 < Q^2 < 0.5$	$0.5 < Q^2 < 1.4$	$0.3 < Q^2 < 0.5$	$0.5 < Q^2 < 1.4$
0.0 –0.04	0.57 ± 0.05	0.61 ± 0.06	0.26 ± 0.03	0.27 ± 0.05	0.14 ± 0.03	0.22 ± 0.07
0.04–0.08	0.50 ± 0.05	0.29 ± 0.04	0.20 ± 0.02	0.17 ± 0.03	0.15 ± 0.03	0.092 ± 0.027
0.08–0.12	0.33 ± 0.04	0.46 ± 0.09	0.12 ± 0.02	0.14 ± 0.03	0.099 ± 0.027	0.140 ± 0.062
0.12–0.16	0.29 ± 0.04	0.19 ± 0.03	0.13 ± 0.02	0.10 ± 0.02	0.069 ± 0.021	0.016 ± 0.009
0.16–0.20	0.14 ± 0.03	0.17 ± 0.04	0.12 ± 0.02	0.13 ± 0.04	0.042 ± 0.016	0.049 ± 0.017
0.20–0.24	0.14 ± 0.03	0.16 ± 0.06	0.074 ± 0.015	0.071 ± 0.020	0.020 ± 0.010	0.103 ± 0.064
0.24–0.32	0.075 ± 0.017	0.155 ± 0.046	0.042 ± 0.009	0.029 ± 0.007	0.016 ± 0.007	0.048 ± 0.016
0.32–0.40	0.079 ± 0.022	0.049 ± 0.014	0.030 ± 0.008	0.027 ± 0.009	0.010 ± 0.007	0.006 ± 0.004
0.40–0.60	0.021 ± 0.006	0.017 ± 0.006	0.010 ± 0.003	0.013 ± 0.004		0.002 ± 0.002
0.60–0.80	0.006 ± 0.003	0.004 ± 0.002	0.003 ± 0.002	0.012 ± 0.005		
0.80–1.0	0.002 ± 0.002			0.002 ± 0.002		

Table 7

$$F(x) = \int_0^{p_{\perp\max}^2} \frac{1}{\pi\sigma_{\text{tot}}} \frac{E^*}{p^*_{\max}} \frac{\Delta^2\sigma}{\Delta x\,\Delta p_\perp^2}\,\Delta p_\perp^2$$

x	$1.5 < W < 1.8$ GeV		$1.8 < W < 2.2$ GeV		$2.2 < W < 2.8$ GeV	
	$0.3 < Q^2 < 0.5$	$0.5 < Q^2 < 1.4$	$0.3 < Q^2 < 0.5$	$0.5 < Q^2 < 1.4$	$0.3 < Q^2 < 0.5$	$0.5 < Q^2 < 1.4$
−1.0–(−0.8)	0.003 ± 0.001	0.006 ± 0.003	0.004 ± 0.001	0.003 ± 0.001	0.002 ± 0.001	
−0.8–(−0.6)	0.016 ± 0.002	0.020 ± 0.005	0.011 ± 0.002	0.015 ± 0.004	0.006 ± 0.002	0.011 ± 0.005
−0.6–(−0.4)	0.034 ± 0.003	0.042 ± 0.007	0.028 ± 0.003	0.024 ± 0.005	0.016 ± 0.002	0.018 ± 0.004
−0.4–(−0.3)	0.033 ± 0.004	0.041 ± 0.009	0.034 ± 0.004	0.045 ± 0.008	0.040 ± 0.004	0.048 ± 0.009
−0.3–(−0.2)	0.052 ± 0.006	0.058 ± 0.011	0.052 ± 0.005	0.063 ± 0.008	0.054 ± 0.005	0.056 ± 0.007
−0.2–(−0.1)	0.050 ± 0.005	0.054 ± 0.012	0.065 ± 0.005	0.090 ± 0.011	0.096 ± 0.006	0.092 ± 0.008
−0.1–0.0	0.072 ± 0.006	0.057 ± 0.008	0.088 ± 0.006	0.081 ± 0.008	0.124 ± 0.007	0.135 ± 0.011
0.0–0.1	0.067 ± 0.006	0.062 ± 0.010	0.084 ± 0.005	0.095 ± 0.009	0.116 ± 0.006	0.117 ± 0.010
0.1–0.2	0.066 ± 0.006	0.068 ± 0.010	0.098 ± 0.006	0.080 ± 0.008	0.106 ± 0.007	0.114 ± 0.010
0.2–0.3	0.059 ± 0.006	0.081 ± 0.012	0.078 ± 0.006	0.071 ± 0.009	0.089 ± 0.006	0.078 ± 0.010
0.3–0.4	0.062 ± 0.006	0.061 ± 0.011	0.068 ± 0.006	0.048 ± 0.005	0.062 ± 0.006	0.056 ± 0.008
0.4–0.5	0.073 ± 0.007	0.055 ± 0.011	0.058 ± 0.006	0.042 ± 0.006	0.047 ± 0.005	0.050 ± 0.008
0.5–0.6	0.073 ± 0.007	0.042 ± 0.007	0.044 ± 0.005	0.026 ± 0.004	0.038 ± 0.005	0.040 ± 0.006
0.6–0.7	0.052 ± 0.006	0.037 ± 0.006	0.047 ± 0.006	0.047 ± 0.014	0.031 ± 0.004	0.038 ± 0.006
0.7–0.8	0.050 ± 0.006	0.044 ± 0.010	0.051 ± 0.006	0.037 ± 0.009	0.030 ± 0.005	0.036 ± 0.009
0.8–0.9	0.016 ± 0.004	0.020 ± 0.009	0.032 ± 0.005	0.025 ± 0.007	0.026 ± 0.005	0.032 ± 0.009
0.9–1.0	0.006 ± 0.003	0.004 ± 0.003	0.015 ± 0.004	0.022 ± 0.010	0.013 ± 0.003	0.022 ± 0.009

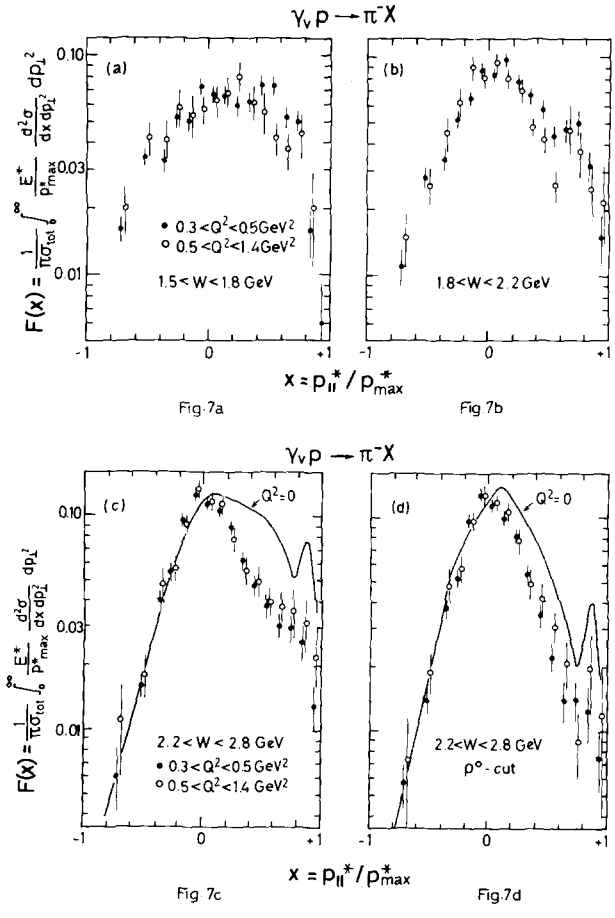

Fig. 7. (a)–(c): The normalised invariant $\pi^- x$ distributions, $F(x)$, for $0.3 < Q^2 < 0.5$ (solid points) and $0.5 < Q^2 < 1.4$ GeV^2 (open points) for three intervals of W. (d): The x distribution of fig. 7c after removal of the quasi-elastic ρ^0 events with normalisation to $\sigma_{tot} - \sigma_{\rho^0}$. The curves in fig. 7c and 7d show the photoproduction data of ref. [5] treated correspondingly.

was made in ref. [13], at Q^2 values up to 6 GeV^2 and values of the scaling variable $\omega = 2\,M\nu/Q^2$ of 2–3, i.e. for deep inelastic collisions. Hence for $Q^2 > 0.3$ GeV^2 the mean charged multiplicity is found to depend only on the energy available and not on details of the production mechanism. The drop in $\langle n_{ch} \rangle$ between $Q^2 = 0$ and $Q^2 = 0.3$ GeV^2 will be discussed in sect. 5.

4. Inclusive distributions

In this section we present inclusive distributions for π^- mesons as a function of the Feynman variable, $x = p^*_\parallel / p^*_{max}$ and of the transverse momentum squared, $p_\perp^2$.

(Here $p_{\parallel}^{*}$ is the longitudinal momentum in the hadronic center of mass system and $p_{\max}^{*}$ the maximum particle momentum kinematically allowed *. The conventional invariant distribution function is used,

$$F(x, p_{\perp}^{2}) = \frac{1}{\pi \sigma_{\mathrm{tot}}} \frac{E^{*}}{p_{\max}^{*}} \frac{\mathrm{d}^{2}\sigma}{\mathrm{d}x\,\mathrm{d}p_{\perp}^{2}},$$

where E^{*} is the particle c.m. energy and we have normalised to the total inelastic $\gamma_{\mathrm{V}}\mathrm{p}$ cross section **. $F(x, p_{\perp}^{2})$ is given for several regions of Q^{2} and W in table 6. In the following we discuss the distributions of x and $p_{\perp}^{2}$.

4.1. x distribution

The x distribution is given by

$$F(x) = \int_{0}^{p_{\perp}^{2}\max} F(x, p_{\perp}^{2})\,\mathrm{d}p_{\perp}^{2}.$$

$F(x)$ is tabulated in table 7 and displayed in fig. 7 for three intervals of W. ***

We observe the following principal features.

(i) The distribution function $F(x)$ increases with W in the central region ($x \approx 0$) due to increasing phase space, i.e. $F(0)$ does not scale.

(ii) $F(x)$ does not change significantly between the Q^{2} regions 0.3–0.5 GeV^{2} (solid points) and 0.5–1.4 GeV^{2} (open points).

(iii) A comparison with photoproduction results [5] (solid curves in fig. 7c,d) for $2.2 < W < 2.8$ GeV shows little difference in the target fragmentation and central region ($x < 0.2$), where the bulk of the events is located. However for $x > 0.2$ we find significantly fewer π^{-} than in photoproduction.

We now examine whether the reduction of π^{-} production at large x is due to a specific channel. The reaction $\gamma\mathrm{p} \to \rho^{0}\mathrm{p}$ is known to be a source of forward π^{-} [5]. In the W interval considered the ratio $\sigma(\gamma_{\mathrm{V}}\mathrm{p} \to \rho^{0}\mathrm{p})/\sigma_{\mathrm{tot}}$ drops by a factor two (from 14% to 7%) between $Q^{2} = 0$ and our Q^{2} range [1]. This effect might be responsible for at least part of the difference between photo- and electroproduction observed in fig. 7c. We have therefore removed in fig. 7d all quasi-elastic ρ^{0} events from

* $p_{\max}^{*}$ has been calculated for a π^{-} recoiling against a $\mathrm{p}\pi^{+}$ system of mass 1.08 GeV.

** Events with visible strange particle decays have been excluded from the total cross section for this procedure.

*** The limited W resolution in the interval $1.5 < W < 1.8$ GeV (see table 1) results in a noticeable smearing of the x value of π^{-} mesons from unfitted events. Most π^{-} in this interval result from the channel $\mathrm{ep} \to \mathrm{ep}\pi^{+}\pi^{-}$ (4C fit). We therefore use kinematic quantities from fitted events $\mathrm{ep} \to \mathrm{ep}\pi^{+}\pi^{-}$ for $1.5 < W < 1.8$ GeV. We estimate the remaining uncertainty of $F(x)$ due to limited resolution to be less than 10%.

the data sample (full and open points) *.

The solid curve of fig. 7d shows the photoproduction data of ref. [5] whose authors used the same cut **. The discrepancy between photo- and electroproduction above $x = 0.2$ although reduced by a factor 1.5 still largely remains. Other known diffractive processes (like diffractive $\gamma_V p \to \omega p$ [2]) are too weak to account for the remaining difference.

Hence we now consider non-diffractive processes which yield π^- in the fragmentation region. The cross sections for $\gamma_V p \to \pi^- \Delta^{++}$ and non-diffractive $\gamma_V p \to \omega p$ determined in this experiment [2,4] show the same drop by a factor 2 between $Q^2 = 0$ and $Q^2 = 0.3$ GeV^2, but are considerably smaller than the ρ cross section and so cannot produce a significant effect. In order to fully explain the Q^2 dependence of $F(x)$ other non-diffractive processes present in photoproduction must develop a Q^2 dependence similar to that of quasi-elastic ρ production.

4.2. $p_\perp^2$ distributions

Fig. 8 shows our $F(x, p_\perp^2)$ distributions for $2.2 < W < 2.8$ GeV and four x intervals. The data are again displayed for $0.3 < Q^2 < 0.5$ GeV^2 (solid points) and $0.5 < Q^2 < 1.4$ GeV^2 (open points). The curves are fits of the form

$$F(x, p_\perp^2) \sim A \exp(Bp_\perp^2 + Cp_\perp^4),$$

to the photoproduction data of ref. [5]. The difference between curve and data points for $0.3 < x < 0.7$ merely reflects the discrepancy of the x distribution noted above. Table 8 shows the results of fits to our data of the form

$$F(x, p_\perp^2) \sim A \exp(-Bp_\perp^2),$$

for $p_\perp^2 < 0.5$ GeV^2. There is no evidence of a change of the slope B with Q^2. Note that the $p_\perp^2$ distributions of fig. 8 for $-0.3 < x < 0.1$ can be equally well decribed by two exponentials with different slopes. The same observation was made in inclusive π^- muoproduction at higher energies [15].

The dependence of $p_\perp^2$ on the variables Q^2, W and x can be seen more clearly in fig. 9 (and table 9) where we show $\langle p_\perp^2 \rangle$ (not weighted by E^*/p^*_{max}) as a function of x for three intervals of W. For $2.2 < W < 2.8$ GeV we compare our data with fits to the photoproduction data of ref. [5]*** (open triangles). Fig. 9 shows the following main features.

* For this purpose $\gamma p \to \rho p$ events were defined as those $\gamma p \to p\pi^+\pi^-$ events with $M_{\pi^+\pi^-} < 1$ GeV. In addition $F(x)$ of fig. 7d is normalised to $\sigma_{tot} - \sigma(\gamma p \to \rho^0 p)$. The number of events removed from the electroproduction data in this way is consistent with our cross sections for $\gamma_V p \to \rho^0 p$.

** The peak in the photoproduction distribution near $x = 0.9$ is due to the reaction $\gamma p \to \pi^- \Delta^{++}$.

*** Ref. [5] tabulates $E^*/\pi p^*_{max}\, d^2\sigma/dx\, dp_\perp^2$. We have removed the E^* dependence using E^* appropriate to each bin center. $\langle p_\perp^2 \rangle$ was then calculated from a fit to the data so obtained.

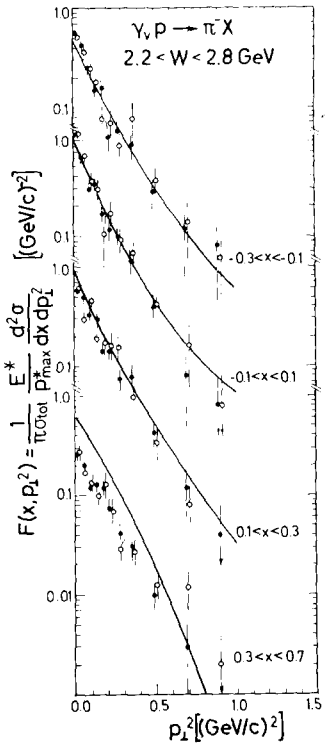

Fig. 8. The invariant $p_\perp^2$ distributions for $\langle W \rangle = 2.5$ GeV are shown for four intervals of x. Solid points show $0.3 < Q^2 < 0.5$ and open points $0.5 < Q^2 < 1.4$ GeV^2. The curves are the fits to the photoproduction data of ref. [5] as described in the text.

(i) $\langle p_\perp^2 \rangle$ increases with W due to the increased phase space available.

(ii) $\langle p_\perp^2 \rangle$ develops with increasing W a characteristic dependence on x with a dip at $x = 0$ (seagull effect).

(iii) At fixed x and W the data show no Q^2 dependence of $\langle p_\perp^2 \rangle$. In particular we find no change in $\langle p_\perp^2 \rangle$ at fixed x when going from photoproduction to our Q^2 range (for $2.2 < W < 2.8$ GeV).

The last observation is further illustrated in fig. 10 where we plot $\langle p_\perp \rangle$ as a function of Q^2 at $\langle W \rangle = 2.5$ GeV and $0.4 \lesssim x \lesssim 0.8$. The open points are from refs. [5,15] It is worth noting that such comparisons should be made at fixed W since $\langle p_\perp \rangle$ is clearly dependent on W, at least for the relatively low W values considered here. For convenience we have also tabulated our $\langle p_\perp \rangle$ results in table 10.

We now discuss the dependence of $\langle p_\perp^2 \rangle$ on x. Firstly the dip at $x = 0$ is caused by an excess of events with small $p_\perp^2$ which manifests itself in a steepening of the $p_\perp^2$ distribution of fig. 8 for small x and $p_\perp^2 < 0.2$ GeV^2. Secondly kinematics forces $\langle p_\perp^2 \rangle$ to

Table 8

Slope of $F(x, p_\perp^2) = \frac{1}{\pi\sigma_{tot}} \frac{E^*}{p^*_{max}} \frac{\Delta^2\sigma}{\Delta x \Delta p_\perp^2}$ for $p_\perp^2 < 0.5$ (GeV/c)^2

x	$1.5 < W < 1.8$ GeV		$1.8 < W < 2.2$ GeV		$2.2 < W < 2.8$ GeV		
	$0.3 < Q^2 < 0.5$	$0.5 < Q^2 < 1.4$	$0.3 < Q^2 < 0.5$	$0.5 < Q^2 < 1.4$	$Q^2 = 0.0$	$0.3 < Q^2 < 0.5$	$0.5 < Q^2 < 1.4$
−0.3–(−0.1)	13.8 ± 1.3	15.0 ± 1.6	8.2 ± 0.7	10.1 ± 0.8	7.0 ± 0.3 [a]	8.8 ± 0.6	9.5 ± 0.8
−0.1–0.1	11.9 ± 1.0	17.0 ± 1.9	10.8 ± 0.6	11.7 ± 1.1	8.8 ± 0.2 [a]	9.2 ± 0.5	8.4 ± 0.5
0.1–0.3	12.2 ± 1.0	15.4 ± 1.3	8.4 ± 0.5	9.9 ± 0.7	7.5 ± 0.2 [a]	7.1 ± 0.4	6.8 ± 0.6
0.3–0.7	14.9 ± 0.9	15.8 ± 1.1	8.5 ± 0.5	8.5 ± 0.7	6.9 ± 0.2 [a]	6.4 ± 0.5	7.1 ± 0.7

[a] Obtained by fitting the data of ref. [5] at $W = 2.48$ GeV.

Table 9
$\langle p_\perp^2 \rangle$ (GeV^2) as a function of x

x	$1.5 < W < 1.8$ GeV		$1.8 < W < 2.2$ GeV		$2.2 < W < 2.8$ GeV	
	$0.3 < Q^2 < 0.5$	$0.5 < Q^2 < 1.4$	$0.3 < Q^2 < 0.5$	$0.5 < Q^2 < 1.4$	$0.3 < Q^2 < 0.5$	$0.5 < Q^2 < 1.4$
−1.0–(−0.8)	0.050 ± 0.019	0.039 ± 0.018	0.083 ± 0.038	0.079 ± 0.043		
−0.8–(−0.6)	0.057 ± 0.013	0.037 ± 0.016	0.080 ± 0.019	0.105 ± 0.057	0.159 ± 0.050	0.101 ± 0.044
−0.6–(−0.4)	0.055 ± 0.009	0.066 ± 0.013	0.102 ± 0.016	0.151 ± 0.050	0.172 ± 0.032	0.134 ± 0.028
−0.4–(−0.2)	0.054 ± 0.007	0.064 ± 0.012	0.094 ± 0.010	0.081 ± 0.009	0.120 ± 0.013	0.138 ± 0.023
−0.2–(−0.1)	0.055 ± 0.009	0.056 ± 0.020	0.077 ± 0.009	0.062 ± 0.009	0.092 ± 0.009	0.093 ± 0.012
−0.1–0.0	0.064 ± 0.008	0.041 ± 0.007	0.069 ± 0.007	0.069 ± 0.009	0.068 ± 0.006	0.083 ± 0.008
0.0–0.1	0.053 ± 0.007	0.039 ± 0.007	0.066 ± 0.006	0.066 ± 0.008	0.082 ± 0.007	0.073 ± 0.008
0.1–0.2	0.060 ± 0.008	0.053 ± 0.011	0.085 ± 0.008	0.068 ± 0.011	0.093 ± 0.009	0.102 ± 0.011
0.2–0.4	0.059 ± 0.006	0.055 ± 0.007	0.100 ± 0.008	0.090 ± 0.010	0.123 ± 0.010	0.127 ± 0.017
0.4–0.6	0.051 ± 0.005	0.063 ± 0.012	0.112 ± 0.012	0.103 ± 0.013	0.125 ± 0.013	0.148 ± 0.024
0.6–0.8	0.045 ± 0.006	0.032 ± 0.005	0.082 ± 0.009	0.080 ± 0.021	0.130 ± 0.017	0.158 ± 0.030
0.8–1.0	0.048 ± 0.015	0.030 ± 0.010	0.060 ± 0.012	0.048 ± 0.014	0.079 ± 0.015	0.106 ± 0.033

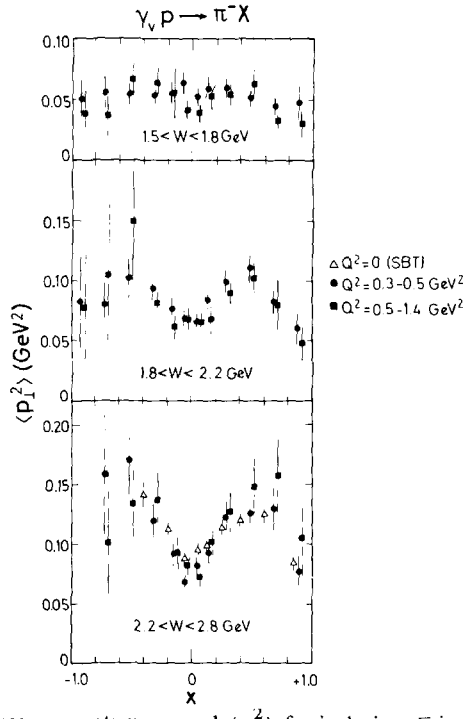

Fig. 9. The mean transverse momentum squared, $\langle p_\perp^2 \rangle$, for inclusive π^- in three intervals of W and two intervals of Q^2. The photoproduction points (Δ) at $2.2 < W < 2.8$ GeV have been deter mined from the data of ref. [5].

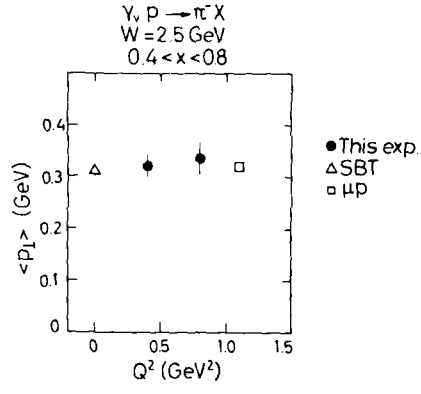

Fig. 10. $\langle p_\perp \rangle$ *versus* Q^2 for $\langle W \rangle = 2.5$ GeV and $0.4 < x < 0.8$, △ photoproduction data [5], ● this experiment and □ ref. [15].

Table 10
$\langle p_\perp \rangle$ (GeV) as a function of x

x	$1.5 < W < 1.8$ GeV		$1.8 < W < 2.2$ GeV		$2.2 < W < 2.8$ GeV	
	$0.3 < Q^2 < 0.5$	$0.5 < Q^2 < 1.4$	$0.3 < Q^2 < 0.5$	$0.5 < Q^2 < 1.4$	$0.3 < Q^2 < 0.5$	$0.5 < Q^2 < 1.4$
−1.0–(−0.8)	0.220 ± 0.080	0.166 ± 0.060	0.251 ± 0.095	0.233 ± 0.097	0.480 ± 0.322	0.149 ± 0.149
−0.8–(−0.6)	0.220 ± 0.044	0.170 ± 0.062	0.254 ± 0.047	0.281 ± 0.115	0.363 ± 0.091	0.292 ± 0.129
−0.6–(−0.4)	0.207 ± 0.027	0.226 ± 0.038	0.276 ± 0.032	0.342 ± 0.085	0.366 ± 0.055	0.321 ± 0.062
−0.4–(−0.2)	0.203 ± 0.020	0.233 ± 0.039	0.269 ± 0.022	0.249 ± 0.025	0.299 ± 0.023	0.324 ± 0.041
−0.2–(−0.1)	0.199 ± 0.024	0.202 ± 0.053	0.229 ± 0.020	0.215 ± 0.029	0.261 ± 0.018	0.256 ± 0.026
−0.1–0.0	0.227 ± 0.022	0.175 ± 0.024	0.221 ± 0.016	0.213 ± 0.021	0.220 ± 0.013	0.242 ± 0.021
0.0–0.1	0.195 ± 0.019	0.167 ± 0.026	0.218 ± 0.016	0.218 ± 0.022	0.241 ± 0.015	0.232 ± 0.020
0.1–0.2	0.213 ± 0.023	0.202 ± 0.035	0.248 ± 0.018	0.223 ± 0.026	0.266 ± 0.019	0.276 ± 0.026
0.2–0.4	0.211 ± 0.017	0.204 ± 0.025	0.276 ± 0.017	0.263 ± 0.025	0.309 ± 0.019	0.311 ± 0.034
0.4–0.6	0.199 ± 0.017	0.229 ± 0.039	0.296 ± 0.025	0.299 ± 0.034	0.316 ± 0.027	0.322 ± 0.037
0.6–0.8	0.187 ± 0.021	0.159 ± 0.025	0.257 ± 0.024	0.309 ± 0.085	0.330 ± 0.038	0.357 ± 0.055
0.8–1.0	0.172 ± 0.038	0.158 ± 0.045	0.220 ± 0.033	0.204 ± 0.058	0.258 ± 0.042	0.285 ± 0.074

decrease close to $x = \pm 1$. These effects result in the "seagull" shape of $\langle p_\perp^2 \rangle$ which has also been observed in inclusive π production with hadron beams. The origin of the excess events in inclusive π^- photoproduction at small $p_\perp^2$ and $x \approx 0$ is twofold: (i) π^- from high multiplicity final states peak at $x \approx 0$ and have much smaller $\langle p_\perp^2 \rangle$ than π^- from low multiplicity final states since less phase space per particle is available (see fig. 19 of fig. [5]), (ii) in photoproduction most of the π^- produced are known to be decay products of parent resonances like ρ, ω, Δ etc. [16–18]. These π^- have considerably smaller x and $p_\perp$ than the parent resonance since the parent momentum must be shared by two or more particles *. This picture has been successfully applied to explain the excess at small $p_\perp^2$ and small x in π^- electroproduction [19].

In *conclusion*: the transverse momentum of electroproduced π^- at fixed W and x shows no dependence on the photon "mass" Q^2 in the range of our experiment. The variation of $\langle p_\perp^2 \rangle$ with W and x can be largely explained by kinematic effects [19].

5. Differences between electro- and photoproduction

In sect. 3 and 4 we have compared our electroproduction data on multiplicity and inclusive π^- distributions with similar data for photoproduction. Although our data show no significant Q^2 dependence over the range 0.3–1.4 GeV^2, there are significant differences from the data at $Q^2 = 0$. The fraction of 1-prongs is higher in electroproduction, resulting in a lower value of $\langle n_{ch} \rangle$. Also there are differences in the $\pi^- x$ distributions. The question now arises whether the difference in $\langle n_{ch} \rangle$ is due to some particular channel, or due to a "conspiracy" of many channels.

The cross section for $\gamma p \to p\rho^0$ is known [1] to fall faster with increasing Q^2 than the total cross section. Similar behaviour occurs for the channels $\gamma p \to \pi^- \Delta^{++}$ and $\gamma p \to p\omega^0$ [2,4]. Nevertheless, these three channels alone cannot account for the difference in $\langle n_{ch} \rangle$ occurring between $Q^2 = 0$ and $Q^2 = 0.3$ GeV^2. At $W = 2.45$ GeV, $\langle n_{ch} \rangle = 2.77$ for photoproduction. If all $p\rho^0$, $p\omega^0$ and $\Delta^{++}\pi^-$ events are excluded $\langle n_{ch} \rangle$ falls to 2.69. This drop of $\langle n_{ch} \rangle$ is only about one third of the difference observed between $Q^2 = 0$ and $Q^2 > 0.3$ GeV^2.

Consequently we must examine other possibilities. If a 1-prong channel plays an important role in the change of $\langle n_{ch} \rangle$ between $Q^2 = 0$ and $Q^2 = 0.3$ GeV^2, the channel involved must be a *multi-neutral* channel. This follows from fig. 11, which shows the missing-mass-squared distributions for the hypotheses $ep \to ep + MM$ and $ep \to e\pi^+ + MM$ for $2.2 < W < 2.8$ GeV. Only few events are found in the neutron and π^0 peaks. Thus the 1-prong channels with one neutral particle in the final state are too small to play an important role in the rise of σ_1/σ_{tot} between $Q^2 = 0$ and $Q^2 \sim 0.3$ GeV^2.

* Note that inclusive ρ^0 production from real photons shows no dependence of $\langle p_\perp^2 \rangle$ on x (for $x < 0.8$), the average $\langle p_\perp^2 \rangle$ being 0.25 ± 0.04 GeV^2 for $W = 2.45$ GeV corresponding to a slope B of 3.7 ± 0.7 GeV^{-2} [16].

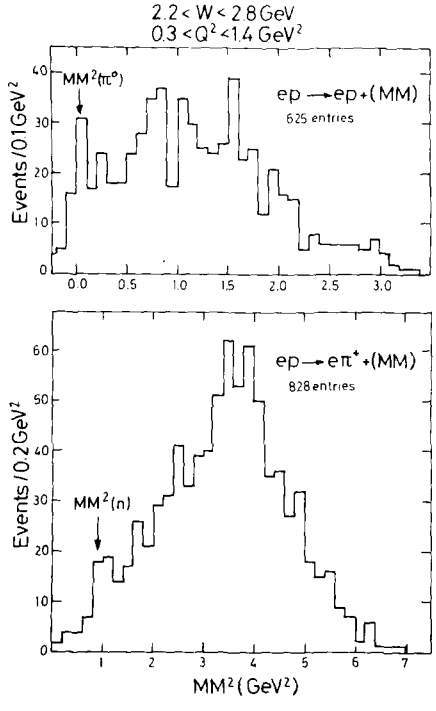

Fig. 11. Missing mass squared distributions for all 1-prong events with $0.3 < Q^2 < 1.4$ GeV^2 and $2.2 < W < 2.8$ GeV. 514 events that fit to both hypotheses, ep → epπ^0 ... and ep → eπ^+n ... are shown with full weight in each plot.

We conclude therefore that the reduction in $\langle n_{ch} \rangle$ between $Q^2 = 0$ and $Q^2 > 0.3$ GeV^2 is (i) not completely explained by the strong Q^2 dependence of ρ^0, ω^0 and Δ^{++} production, and (ii) if due to a relative increase of the 1-prong cross section, must originate from the channels ep → eπ^+ + X or ep → ep + X, where X represents two or more missing neutrals.

6. Conclusion

We have studied the inclusive features of electroproduction as a function of the variables Q^2, W, x and $p_\perp$. No significant Q^2 dependence of the mean charge multiplicity $\langle n_{ch} \rangle$, fractional prong cross section σ_n/σ_{tot} or π^- inclusive x distribution is observed over the range $0.3 < Q^2 < 1.4$ GeV^2, studied in this experiment. In contrast, significant differences are seen compared to photoproduction data at $Q^2 = 0$. It appears that this behaviour is not due to the influence of only one or two specific channels with a Q^2 dependence different from the majority of channels. The $p_\perp^2$ distributions for inclusive π^- have been examined and compared with photoproduction

results. There is no evidence for a change of $\langle p_T^2 \rangle$ as Q^2 increases (figs. 9 and 10). This contradicts the shrinkage behaviour expected in some theories [20].

We thank I. Bloodworth, B. Naroska, D. Notz and W.J. Podolsky for their contributions in the early stages of this experiment. We are indebted to N. Gollmer, E. Hell, V. Heynen, A. Huber, K. Klinkmüller, G. Kraft, H.H. Sabath, S.W. Sass, K. Westphal and K.H. Wroblewski for technical assistance. The excellent performance of the Synchrotron crew, of the Hallendienst and of the Kältetechnik is gratefully acknowledged. We want to thank our scanning and measuring personnel for their careful work. The cooperation by Mr. Kuhlmann and the Rechenzentrum has been very helpful.

The work at Hamburg has been supported by the Bundesministerium für Forschung und Technologie. The work at Glasgow has been supported by the Science Research Council.

References

[1] P. Joos et al., Nucl. Phys. B113 (1976) 53.
[2] P. Joos et al., Nucl. Phys. B122 (1977) 365.
[3] V. Eckardt, H.J. Gebauer, P. Joos, H. Meyer, B. Naroska, D. Notz, W.J. Podolsky, G. Wolf, S. Yellin, H. Dau, G. Drews, D. Greubel, W. Meincke, H. Nagel and E. Rabe, Nucl. Phys. B55 (1973) 45;
V. Eckardt et al., DESY report 74/5 (1974);
E. Rabe, Thesis, DESY internal report F1-74/2 (1974), unpublished.
[4] K. Wacker, Thesis, DESY internal report F1-76/04 (1976), unpublished.
[5] SLAC-Berkeley-Tufts Collaboration, Phys. Rev. D5 (1972) 1603; SLAC-PUB-1004 which contains tables of the data.
[6] S. Stein, W.B. Atwood, E.D. Bloom, R.L.A. Cottrell, H. DeStaebler, C.L. Jordan, H.G. Piel, C.Y. Prescott, R. Siemann and R.E. Taylor, Phys. Rev. D12 (1975) 1884.
[7] L. Hand, Phys. Rev. 129 (1964) 1834.
[8] SLAC-Berkeley-Tufts Collaboration, Phys. Rev. D5 (1972) 545; D8 (1973) 1277.
[9] T.A. Armstrong, W.R. Hogg, G.M. Lewis, A.W. Robertson, G.R. Brookes, A.S. Clough, J.H. Freeland, W. Galbraith, A.F. King, W.R. Rawlinson, N.R.S. Tait, J.C. Thompson and D.W.L. Tolfree, Phys. Rev. D5 (1972) 1640.
[10] Aachen-Berlin-Bonn-Hamburg-Heidelberg-München Collaboration, Phys. Rev. 175 (1968) 1669;
H. Spitzer, DESY internal report F1-71/4 (1971).
[11] C. del Papa et al., Phys. Rev. D13 (1976) 2934.
[12] J. Ballam, E.D. Bloom, J.T. Carroll, G.B. Chadwick, R.L.A. Cottrell, M. Della Negra, H. DeStaebler L.K. Gershwin, L.P. Keller, M.D. Mestayer, K.C. Moffeit, C.Y. Prescott and S. Stein, Phys. Lett. 56B (1975) 193.
[13] P.H. Garbincius, K. Berkelman, B. Gibbard, J.S. Klinger, P. Wanderer and A.J. Sadoff, Phys. Rev. Lett. 32 (1974) 328;
B. Gibbard et al., Phys. Rev. D11 (1975) 2367.
[14] V. Blobel, A. Eskreys, H. Fesefeldt, H. Franz, K. Von Holt, U. Idschok, J.W. Lamsa, R. Rödel, N. Schmitz and W. Treffeisen, Nucl. Phys. B92 (1975) 221.

[15] C. del Papa et al., Phys. Rev. D15 (1977) 2425.
[16] E. Kogan et al., Nucl. Phys. B122 (1977) 383.
[17] W. Struczinski et al., Nucl. Phys. B108 (1976) 45.
[18] W.J. Podolsky, Thesis, Lawrence Radiation Lab. report UCRL-20128, Berkeley, 1971.
[19] A. Seiden, Phys. Lett. 68B (1977) 157; SLAC-PUB-1962, Nucl. Phys. B, submitted.
[20] H. Cheng and T.T. Wu, Phys. Rev. 183 (1969) 1324;
J.D. Bjorken, J. Kogut and D. Soper, Phys. Rev. D2 (1971) 1382;
H.T. Nieh, Phys. Lett. 38B (1972) 100.